Chapter 3 Development of a Finite Element Model of the Test Cavity System

The test cavity system has been built in order to investigate the mechanisms and feasibility of global active noise control in an enclosure similar in size and shape to a Ford Explorer (Figure 3.1). The system characteristics (rigid boundary conditions, shape and dimensions) have been chosen in order to model approximately the acoustic dynamics of the interior cabin of the car.

A side view of the cavity is shown in 3.1 with its dimensions given in meters. As illustrated in Figure 3.2, the cavity is made of particle board reinforced with wooden beams. This design has been chosen in order to make the walls of the enclosure as rigid as possible (mostly rigid boundary conditions simplify the model). A steel plate (Table 3.1) has been clamped to the cavity and a shaker attached to the plate provides the excitation force, as shown in Figure 3.2. The position of the plate is roughly the same as the position of the firewall in the Ford Explorer, because it was thought to be one source of noise in the car. However the properties of the plate are different of those of a typical automobile firewall. It is very difficult to obtain "clamped" boundary conditions experimentally. In order to approximate these conditions as well as possible, the steel plate was sealed and screwed to the rest of the structure at ten positions along its length and twenty five along its width. The noise field is created by the radiation of the plate inside the cavity. The plate has been positioned as in Figure 3.2 in order to simulate the vibration of the firewall of the car. The vibration of the firewall was thought to be the most dominant source of noise in the cabin of the car, especially when the engine was running (see later). The positions of the four control sources are also shown in Figure 3.2. The sources are 9" diameter commercially available audio speakers. A door was placed on the left side of the structure because access to the interior of the cavity was required to change the

position of the error sensors in the numerous control configurations. Test results are discussed in section 4.3 Active Noise Control Experimental Results with Optimized Configuration.

For the numerous control experiments and modal analyses, a scanning system for the pressure field inside the cavity was required. A grid of microphones mounted on a moving vertical plane was built to scan the interior volume. Figure 3.3 shows the grid and the positions of the thirty PCB microphones. During the scanning, the traverse is manually moved from the back to the front of the cavity for ten axial positions. These positions are shown in Figure 3.1.

The finite element model has been developed in three stages. First, the acoustic behavior of the cavity was studied (section 3.1); second, a model for the disturbance was developed (section 3.2); third, the model of the disturbance was applied to the acoustic model of the cavity (section 3.2).

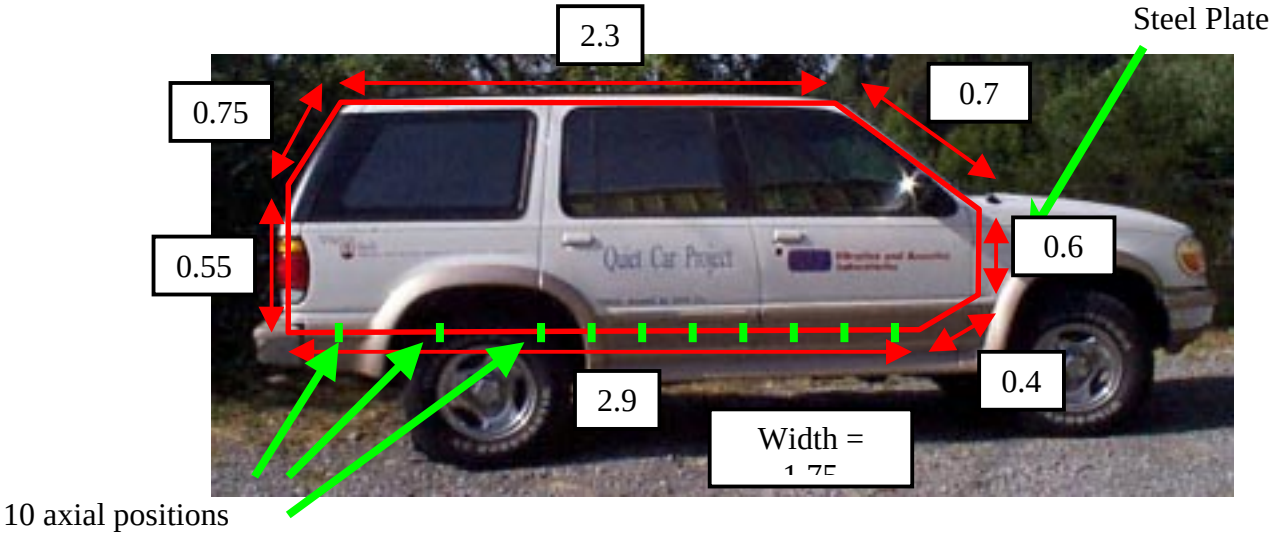

Figure 3.1 Side view of the test cavity system with dimensions

Table 3.1 Characteristics of the disturbance plate

Height	0.6 m
Length	1.8 mm
Width	3.175 mm
Density	7700 kg m^{-3}

Young's Modulus	19.5 e10 Pa
Characteristic Impedance	47.0 e6 Pa s m^{-1}
Poisson's Ratio	0.28

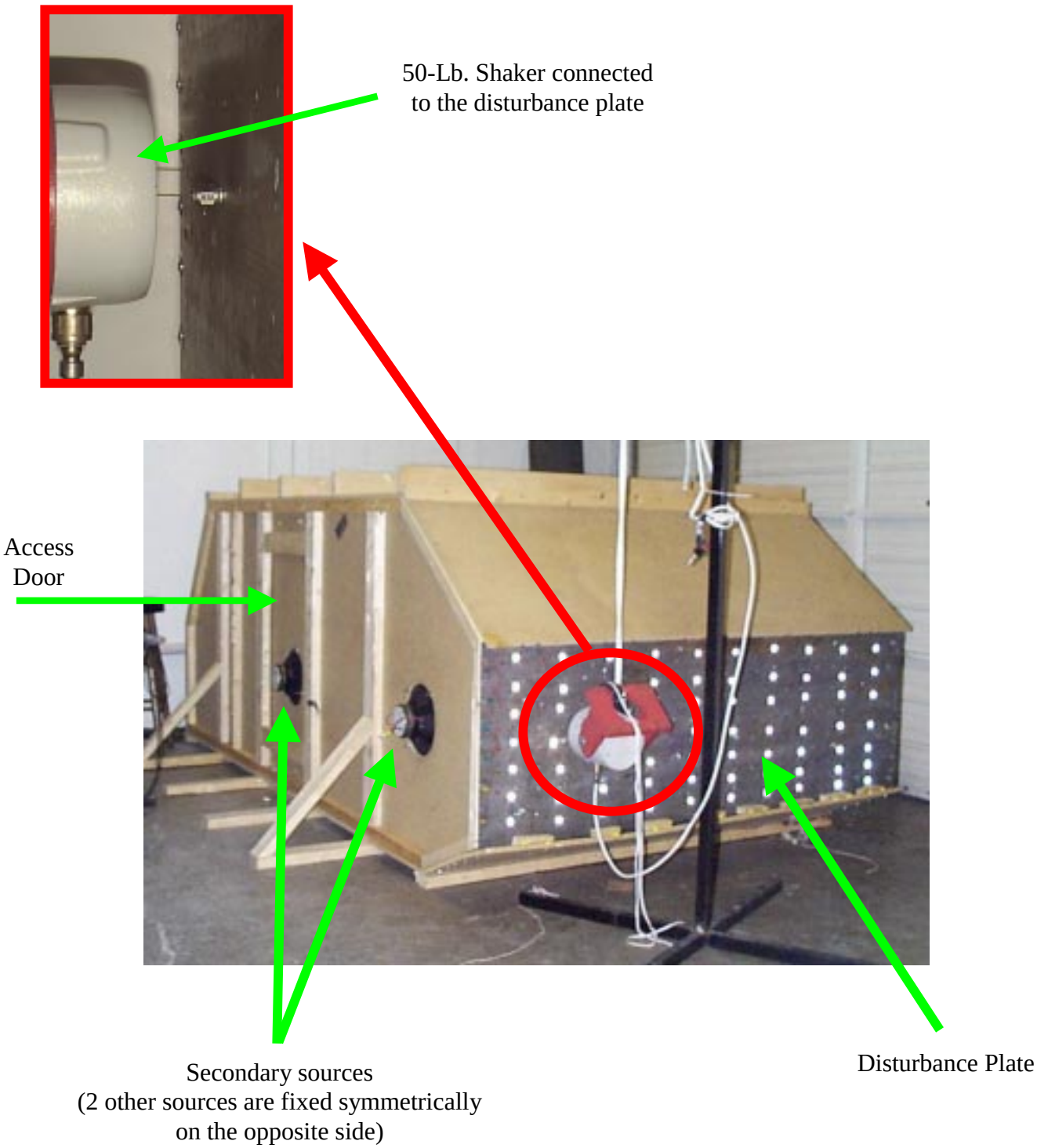

Figure 3.2 General view of the test cavity system

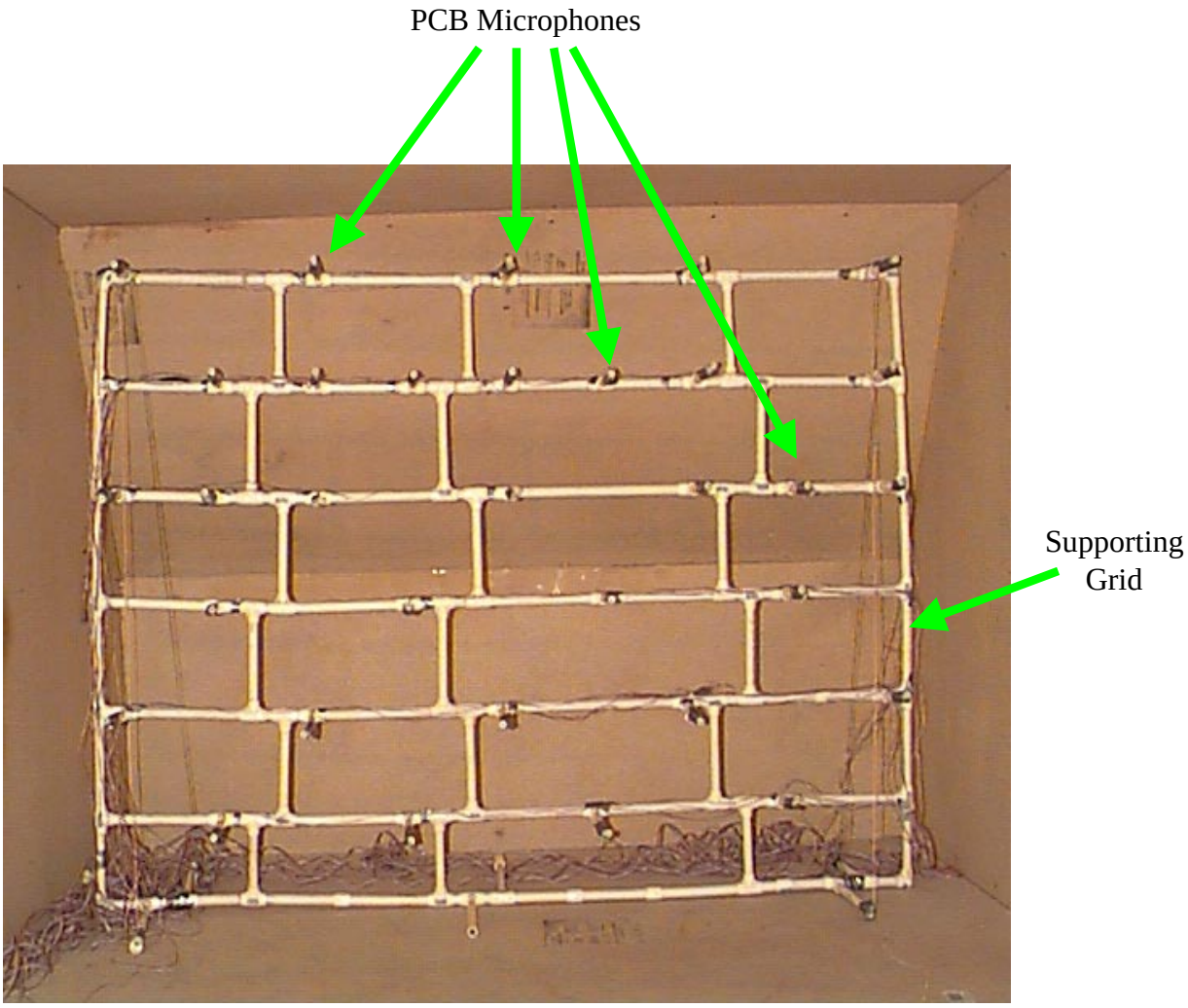

Figure 3.3 View of the cavity interior with measurement system

3.1 Acoustic Analysis of the Cavity

The acoustic dynamics of the cavity are fully described by three parameters: the natural frequencies, the mode shape and damping associated with each natural frequency. These three parameters can be extracted experimentally or obtained with the knowledge of the dimensions, shape and boundary conditions of the test cavity, as well as the characteristics of the fluid (Air at 25 C, in this case). Note however, that analytically obtaining the damping associated with each mode is not straightforward.

The acoustic modal analysis was performed both experimentally and with the model. In order to ensure the accuracy of the model, the natural frequencies and mode shapes it provides must compare well with those measured experimentally. If this is so, the modal damping extracted from the experimental data can be added to the model.

3.1.1 Experimental Acoustic Modal Analysis of the Test Cavity system

Three modal parameters that can be extracted from the experimental modal analysis fully describe the dynamics of the cavity:

- Natural Frequencies (ω_n)
- Modal Damping coefficients (ζ_n)
- Mode Shapes (Φ).

The algorithm used to extract these parameters is based on a frequency domain curve fit of the transfer function H(ω) between the pressure measured at point i inside the cavity and the velocity measured at point k (location of the speaker used to create the pressure field) [52]. The transfer function can be expressed by modal superposition, in terms of the modal parameters:

$$H_1(\omega) = \frac{P_i}{V_k}(\omega) = \sum_{Modes} \frac{\Phi_{im}\Phi_{km}}{M_m(\omega_m^2 - \omega^2 + 2\xi_m\omega\omega_m)}, \tag{3.1}$$

where M_m is the modal mass, ω_m is the natural frequency, ζ_m is the damping of mode m and ϕ_{tm} is the modal participation of mode m at point i. The mode shapes are proportional to the modal participation:

$$\begin{Bmatrix} Modeshape_m(x_1) \\ \cdots \\ Modeshape_m(x_k) \\ \cdots \end{Bmatrix} = \alpha_m \begin{bmatrix} \Phi_{m1}\Phi_{mk} \\ \cdots \\ \Phi_{mk}\Phi_{mk} \\ \cdots \end{bmatrix}, \tag{3.2}$$

where α_m is the coefficient of proportionality for the mode m.

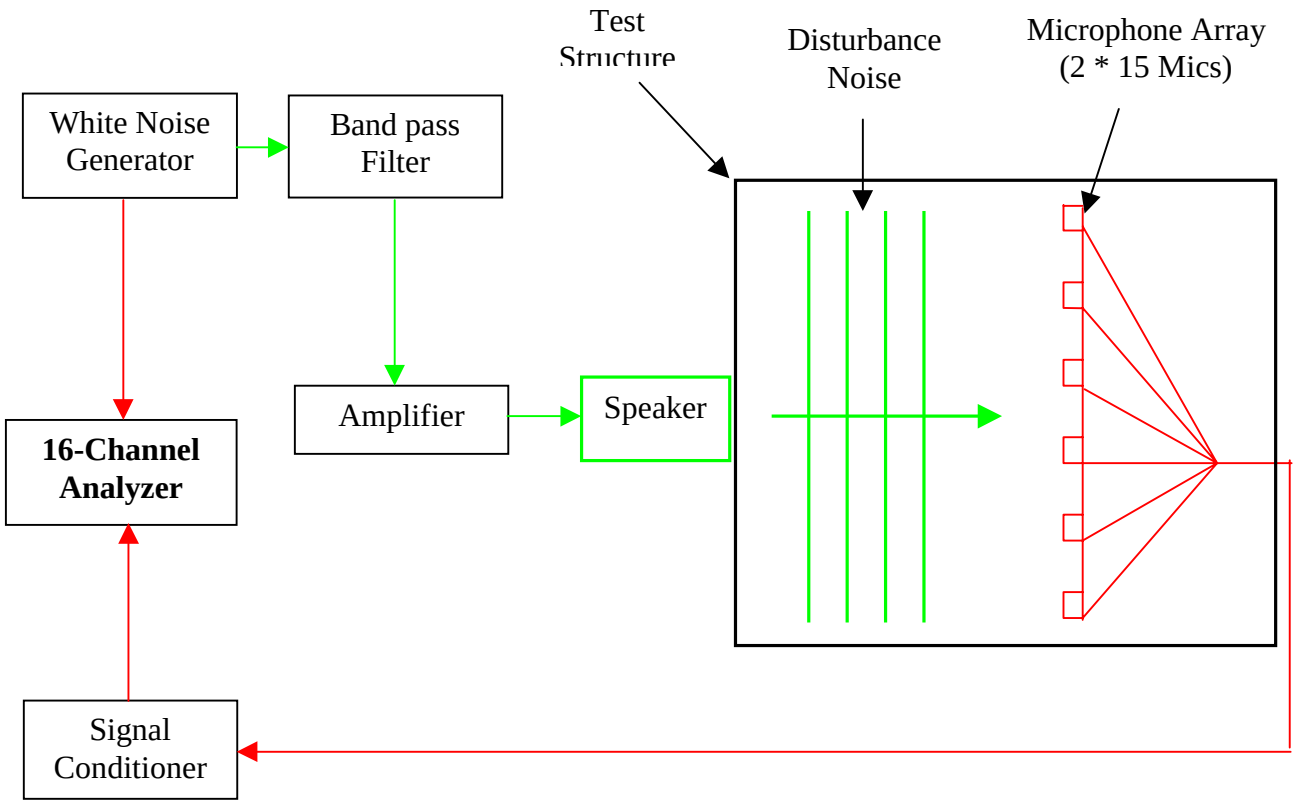

Figure 3.4 Schematic of measurement system

The system presented in Figure 3.4 is used to perform the acoustic modal analysis. Since the interest is limited to low frequencies, the signal from a white noise generator is band pass filtered between 30 and 300 Hz by Ithaco filters (24 dB per octave roll-off, model 4302). A 6-channel Rane amplifier adjusts the level of the signal received by the loudspeaker (9" subwoofer) to acoustically excite the cavity. The loudspeaker was located in the lower right corner in the

back of the cavity. Because of the rigid boundary conditions there is no node at this location, and the speaker can therefore excite all the modes. The signals of 30 PCB acousticel Type 130A microphones are acquired with a 16 channel digital analyzer linked to a PC for post processing. Due to the number of channels available on the analyzer, the acquisition has to be repeated twice for each position of the traverse. The band pass filtered white noise is connected to channel 1, while microphones 1 to 15 (then 16 to 30) are connected to channel 2 to 16. The analyzer computes the auto spectrum of each channel as well as the cross spectrum between channel 1 and channels 2 to 16. This information is required for computation of both the transfer function H_1 and the coherence ν (used in the curve fit algorithm),

$$H1 = \frac{Gab}{Gaa} \tag{3.3}$$

$$\nu = \frac{Gab^{2}}{Gaa * Gbb} \tag{3.4}$$

The results of the analysis are presented in Table 3.2 and Figures 3.5 and 3.6, which respectively give the natural frequencies, magnitude, and phase of the mode shapes. Table 3.2 shows that the modal density is high at frequencies as low as 150 Hz. Around this frequency three modes appear within 12 Hz, while four modes appear within 8 Hz around 200Hz. The number of participating modes at a frequency represents the number of degrees of freedom of the system at that particular frequency. In order to control a system with n degrees of freedom, n active sources are required. Due to the bunching of the modes at 150 Hz and above, the dimensions of the control system needed to achieve global control of the cavity must be large. The results obtained with this first analysis indicate that four control actuators are required to perform global control at frequencies higher than 150 Hz. This is so because at those frequencies the number of modes that contribute to the response is greater than four. At lower frequencies, close to resonance, the response is dominated by one mode, therefore, a lower number of control channels can be used to control lower frequencies.

Table 3.2 Acoustic modal parameters

Natural Frequency (Hz)		Damping
F.E.Model	**Experiment**	
58	60	0.05
99	105	0.021
114	120	0.025
114		
151	154	0.012
158	159	0.035
163	165	0.035
183	182	0.02
186	186	0.02
191	189	0.012
200	200	0.005
203	202	0.01
208	208	0.007
208	211	0.007
226	227	0.012
230	231	0.005
236	233	0.012
240	245	0.012
251	255	0.012

Due to the simplified shape of the test cavity, most of the mode shapes are very similar to those of a rectangular box. As illustrated in Figure 3.5, mode 1 shows a nodal plane perpendicular to the x-axis and crossing the cavity at its middle. The pressure amplitude is constant along the y-z plane. Mode 2 shows a similar nodal plane perpendicular to the y-axis,

and a general shape similar to the shape of mode 1. The amplitude of the pressure is constant along the x-z plane. The shape of mode 3 is very different from the shape of the third mode of a rectangular box. Experimentally, mode 3 shows two curved modal surfaces as illustrated in Figure 3.5 (c). As it will be shown later in the analysis conducted with the model, mode 3 has two nodal planes perpendicular to the x-axis, and the amplitude of the pressure is constant along the y-z plane. A discussion on the differences between the experimentally extracted and theoretical mode shape will be given in the following section. In a real car, the damping associated with the modes is higher than in the model, but the general trends regarding the mode shapes are the same. The natural frequencies are similar because the shape, dimensions and boundary conditions of the car are close to those of the model.

Mode shapes also provide information concerning strategy of location of control sources. In order for the control source to be well coupled with the acoustic fluid, it has to be located as close as possible to an antinode. For example, the global control of mode 1 could be achieved by locating one source in the plane perpendicular to the x-axis and at the very end of the cavity. As illustrated in Figure 3.5 (a) the pressure amplitude is maximum at this position and therefore the source would couple well into the acoustic fluid for the control of this particular mode. Nevertheless, in the case presented in this thesis, the assigned goal is the global control of the enclosure in a large bandwidth. As illustrated in Table 3.2, in the frequency band considered (40 to 250 Hz) there are nineteen modes, and therefore a fixed set of actuators (i.e. four actuators in the case presented in chapter 4) can not couple well into all these modes. It can be concluded then that knowledge of the modes is not sufficient to define the locations of the control sources for global control of the test cavity between 40 and 250 Hz. An optimization technique has to be used to minimize the energy in the cavity with the constraint that only four control actuators can be used. The technique chosen is the genetic algorithm (detailed in section 4.2). The algorithm will minimize the acoustic potential energy in the cavity between 40 and 250 Hz by changing the locations of the four control sources and computing the energy for each configuration of actuators.

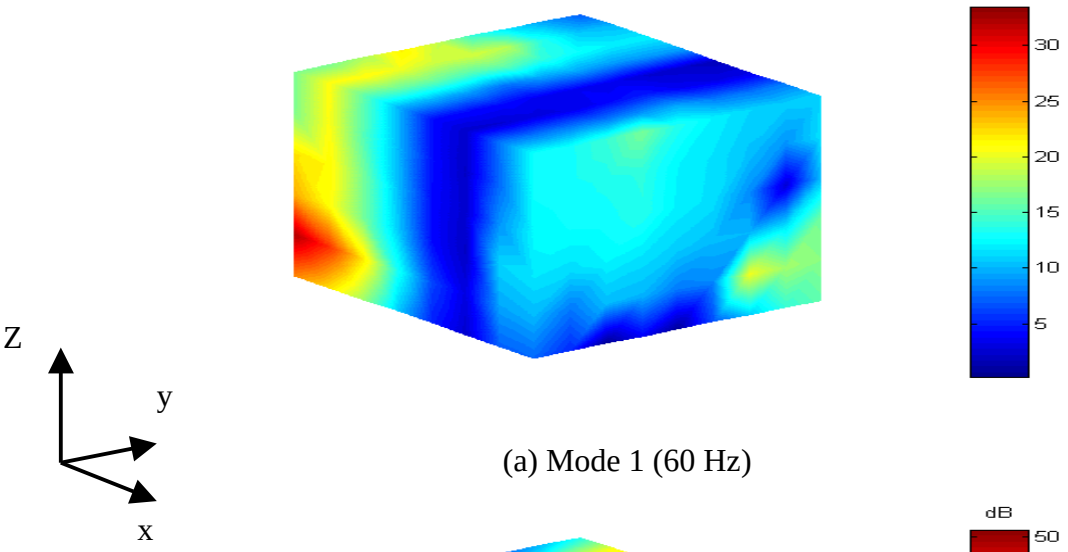

(a) Mode 1 (60 Hz)

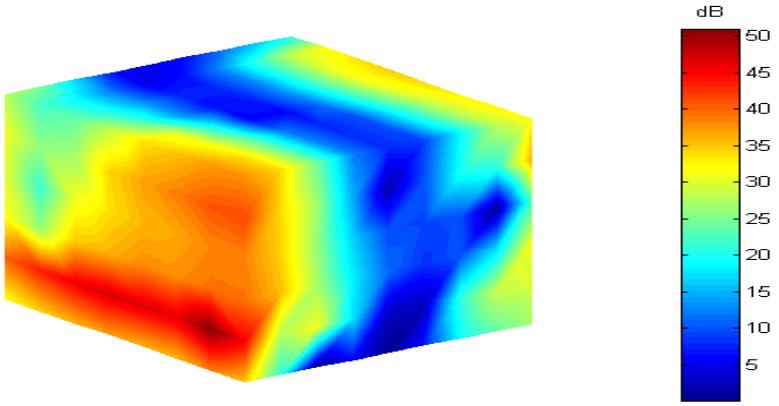

(b) Mode 2 (99 Hz)

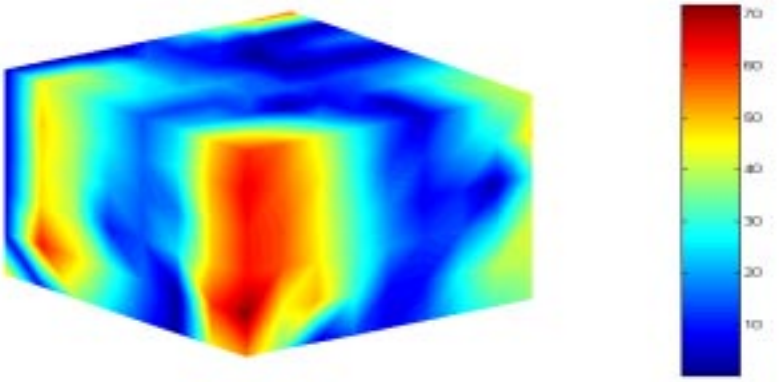

(c) Mode 3 (120 Hz)

Figure 3.5 Experimental acoustic mode shapes (magnitude)

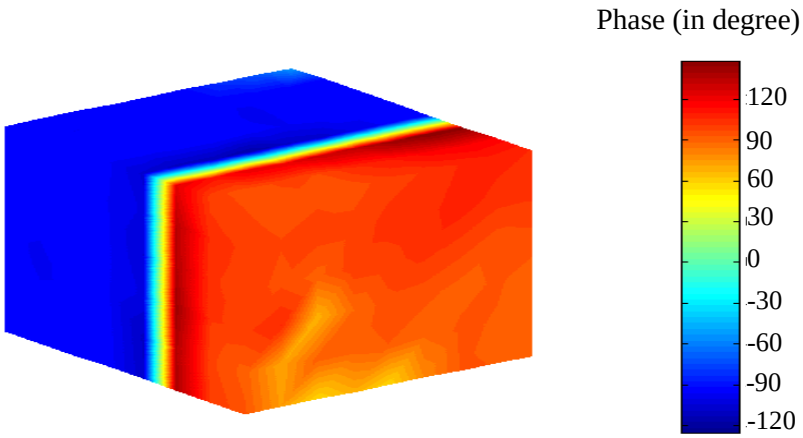

(a) Mode 1 (60 Hz)

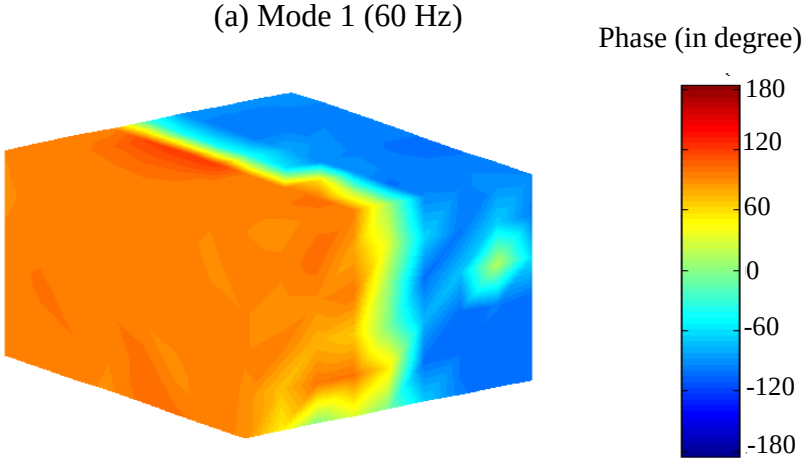

(b) Mode 2 (99 Hz)

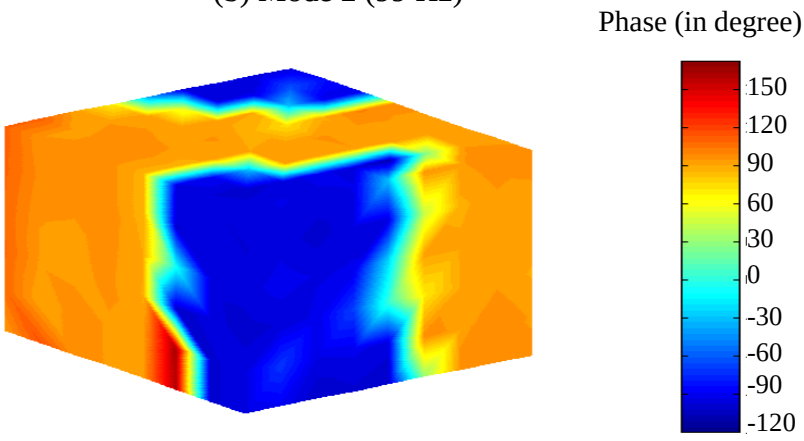

(c) Mode 3 (120 Hz)

Figure 3.6 Experimental acoustic mode shapes (phase)

3.1.2 Modal Analysis using the Finite Element Model

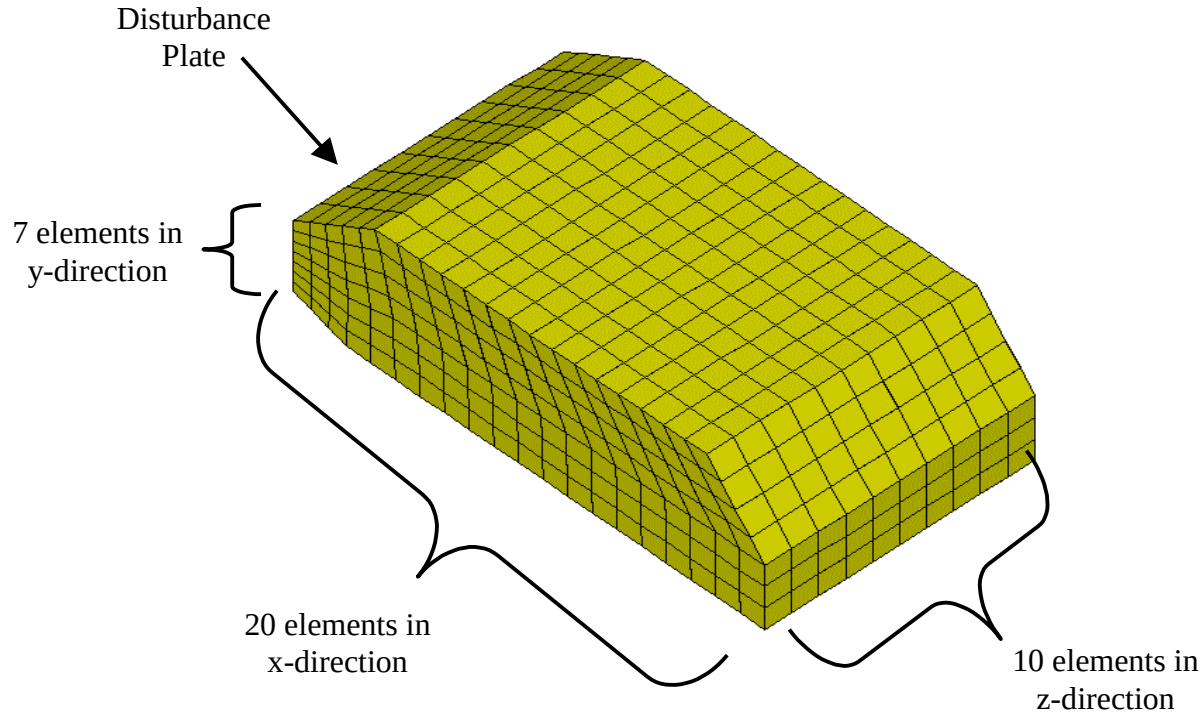

Figure 3.7 Finite element model

The geometry of the finite element model presented in Figure 3.7 has been designed using I-DEAS [53]. This geometry was then imported into the Sysnoise [41] finite element package for acoustic analysis. The elements used for the meshing task are "rectangular bricks", which have one node per corner. The density of the elements has been calculated using eight elements per wavelength to give a maximum frequency of 250 Hz for which the model is valid. The accuracy of the results provided by a finite element model depends on the number and type of elements that are used to grid the volume of the cavity. When experimental knowledge of the cavity is available, the results provided by the model can be compared to the results obtained experimentally, therefore making it possible to check the validity of the model. If no experimental knowledge of the test cavity is available, there is no guarantee that the results of the model will be accurate. To overcome this problem, a convergence study on the number of elements to be used is necessary and should be performed.

A typical convergence study proceeds as follows: the pressure inside the cavity are then computed for models with an increasing number of elements. The results obtained with the different models should be compared. Increasing the number of elements will increase the accuracy of the model until a certain number of elements is reached. Increasing the number of elements beyond this number should not affect the results. This number is the minimum number of elements to be used in the model.

The finite element model was developed in two steps. First, with a knowledge of the dimensions of the test cavity and the characteristics of the fluid (air at 25° C), the natural frequencies and mode shapes were computed using Sysnoise. These results are also presented in Table 3.2. Figures 3.8 and 3.10 show respectively the magnitude and phase of the first three modes. Note that the results obtained experimentally are very similar to those obtained with the model. In terms of natural frequency, the largest difference occurs at 114 Hz where the absolute difference is 6 Hz (5%). At higher frequencies, the model agrees very well with the experiment. Around 200 Hz, the difference is of the order of 1%, which is negligible due to the uncertainties in the experimental data.

The first mode shapes have been compared, and the same trends are observable in the model and the experiment. This is shown in Figures 3.5 and 3.8, which represent the magnitude of the mode-shapes obtained experimentally and with the finite element model, respectively. The phase of the mode shapes are shown in Figure 3.6 and 3.10, obtained experimentally and with the finite element model, respectively. Modes 1 and 2 have the shape of the modes of a rectangular box, comparable to those extracted experimentally. The nodal plane appears at the same locations and the pressure is constant in the directions parallel to the nodal plane. Modes 3 and 4 appear at the same frequency; the shape of these modes is also the same as those of a theoretical rectangular box. They both have two nodal surfaces. In the case of mode 3, they are parallel to each other and perpendicular to the x-axis. In the case of mode 4, they are perpendicular to each other and the x and y-axis. Experimentally only one mode was extracted at 120 Hz, but with a different mode shape. This is due to the limit of the experimental extraction method. Computation of the pressure distribution at 114 Hz using the model (Figure 3.9 and 3.11) shows the same trend as the experimental data. The experimentally extracted mode is the superposition of the two modes computed using the model. In conclusion, very good agreement was obtained between the model and the experimental set up.

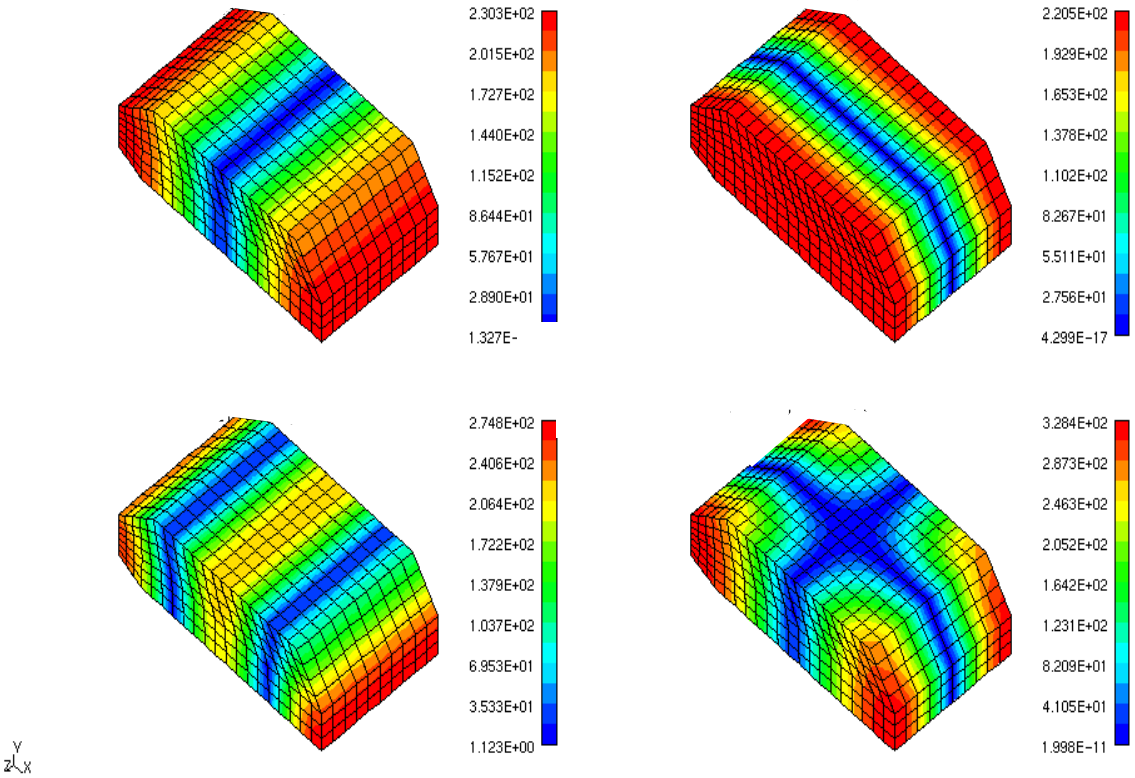

Figure 3.8 FEM mode shapes (magnitude)

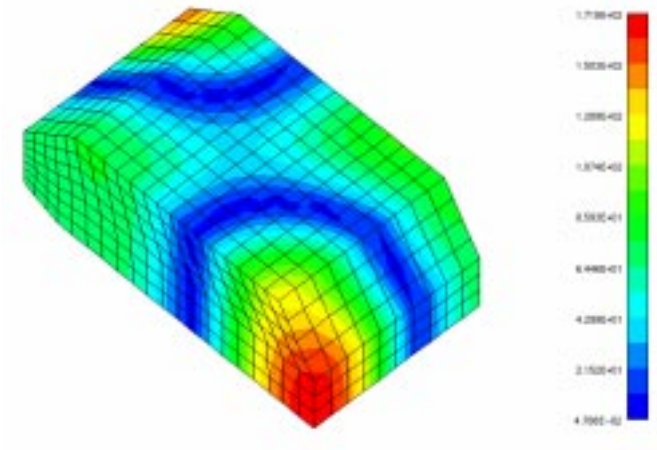

Figure 3.9 Pressure distribution at 114 Hz (magnitude)

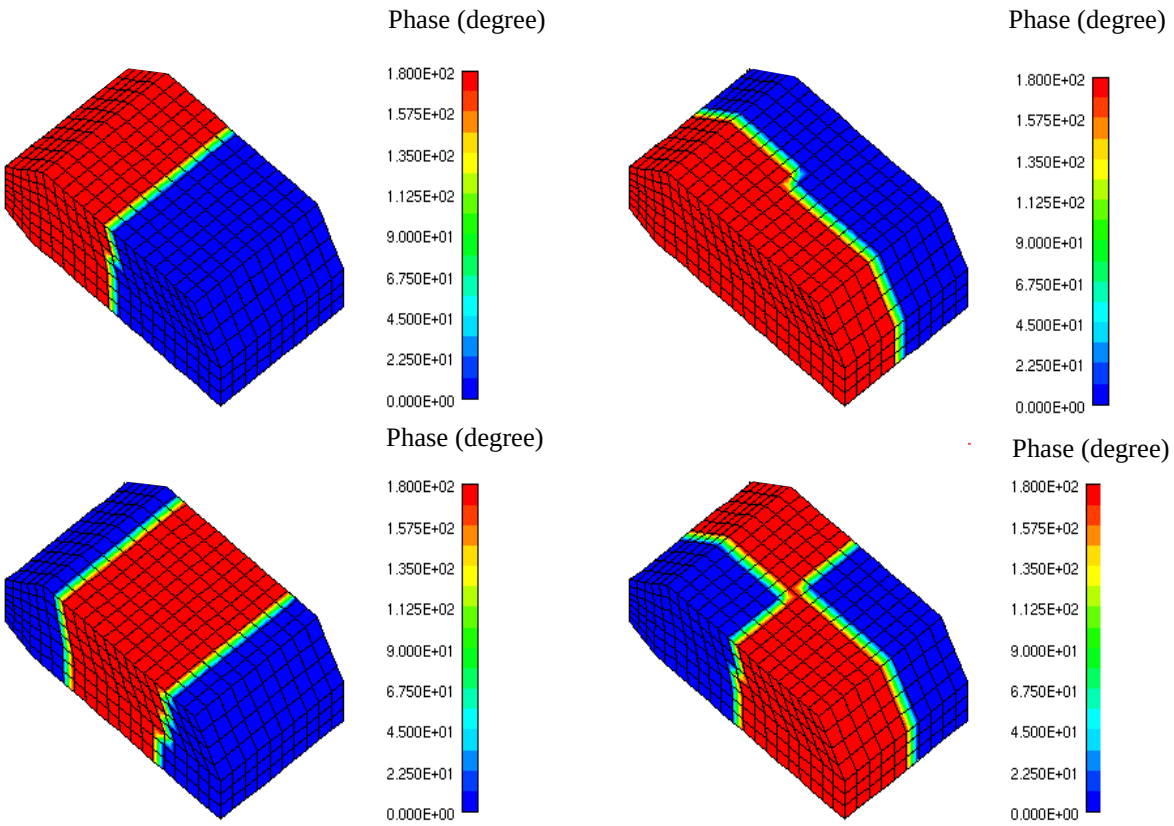

Figure 3.10 FEM mode shapes (phase in degrees)

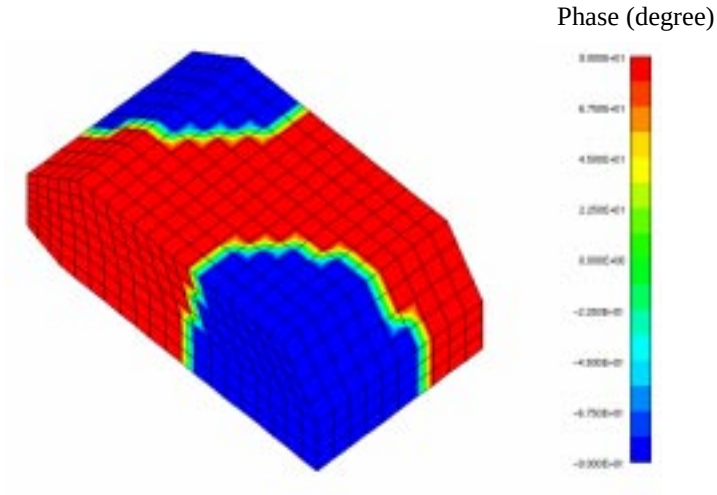

Figure 3.11 Pressure distribution at 114 Hz (phase in degrees)

Second, the model was updated with the modal damping that was measured experimentally. This damping was extracted by curve fitting, as described in section 3.1.1. The software package offered the option to define the damping associated with each of the modes previously computed. The effect of the damping was to decrease the amplitude of each of the peaks occuring at the resonance frequencies, and also to decrease the quality factor at these frequencies. Figure 3.12 presents the frequency response averaged at microphones located on the scaning system. It can be seen that the amplitude of the peaks varies from 15 dB at 120 Hz, down to 3 dB at 190 Hz. Due to the damping (i.e. the quality factor) and the close-together resonance frequencies, a sharp peak does not occur at each of the natural frequencies. For example, although three resonance frequencies have been extracted (151, 158 and 163 Hz), there is only one peak at 150 Hz.

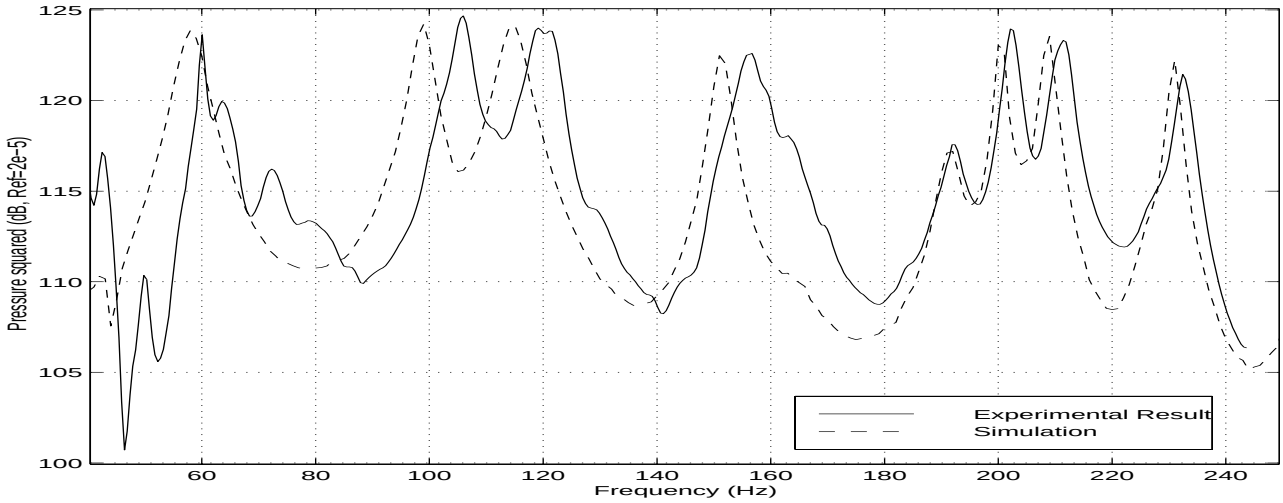

Figure 3.12 Frequency response

3.1.3 Conclusions

The experimental acoustic modal analysis conducted on the test structure permitted validation of the acoustic finite element model. The natural frequencies and mode shapes obtained with the two approaches were very similar, and experimental modal damping has been integrated into the finite element model. As a conclusion and last validation, the frequency response at the microphones (mounted on the traverse, as in Figure 3.3) due to a speaker located on the side of the test structure has been computed with the finite element model. In this computation, the speaker is modeled as a rectangular piston of the same surface area as the speaker. This is justified by the fact that a speaker has its entire surface vibrating in phase with a similar amplitude in the low frequency band of interest for this application. Considering the low frequency approximation, it was thought that the difference in shape the speaker being circular and the element rectangular, would be neglible. The sum of the pressure squared computed at 300 sensors for both the experiment and the simulation is presented in Figure 3.12. Experimentally, the sensors are those mounted on the vertical grid presented in Figure 3.3, which was positioned at the ten axial positions as shown on Figure 3.1. In the model, the pressure was taken at the nodes corresponding to the location of these sensors. Note from the figure that the trends are very similar from 80 to 250 Hz, which encompasses most of the frequency band of interest. Nevertheless, the frequency response is somewhat different at very low frequencies, between 40 and 70 Hz. Two peaks appear between 40 and 60 Hz, and one peak appears between 60 and 70 Hz in the experimental data. According to the modal analysis, these peaks do not represent acoustic modes of the cavity since the natural frequencies are similar in the model and in the experiment. Most likely they are caused by structural resonances, resulting from non-rigid boundaries at those frequencies. Recall that the boundaries of the experimental cavity are made of particle boards, and an access door is simply screwed to the rest of the structure. The vibration of these panels has not been studied.

3.2 Analysis of the velocity field of the disturbance plate excited by a point force

As mentioned earlier, the disturbance field in the test cavity is created by the vibration of a steel plate (Table 3.2) attached to the front end of the test structure. A 50-lb. shaker attached to the plate by a stinger applies a point force at the position shown in Figure 3.2. In a first experiment, the modal analysis of the plate without the shaker has been conducted. As described previously, the analysis provides the mode shapes and natural frequencies of the plate. In a second experiment, the velocity of the plate created by the disturbance force has been measured using a laser vibrometer. Using the known mode shapes, the number of wavelengths in the x and y directions can be determined for each mode. Considering that two data points per wavelength are necessary to obtain an accurate model of the vibration field, the number of positions necessary to accurately approximate the velocity field of the plate can be determined.

3.2.1 Experimental Modal Analysis of the Disturbance Plate

In the case of the vibration modal analysis of the plate, the strategy is the same as in the case of the acoustic modal analysis of the test cavity presented in section 3.1.1. The only difference is the equipment used. As illustrated in Figure 3.13, the excitation of the plate is obtained by an impact force provided by a PCB modal hammer. The hammer has a force transducer attached to it. The excitation of the plate is measured by a PCB mini-accelerometer mounted on the plate. The signals from the accelerometer and the force transducer are gained and input to a B&K 2-channel analyzer. The analyzer computes the transfer function between the force and acceleration for frequencies below 400 Hz, with a 0.5 Hz resolution. The set up of the analyzer is described in table 3.3. The acquisition of the signals is triggered by an increasing force equal to ten percent of the maximum force. The signals are windowed with a two-second exponential window and five averages are used to compute the transfer function. During the analysis the accelerometer was fixed, and impulses were applied to the structure at evenly spaced locations (192 points were used; 8 lines of 24 points). Since the accelerometer was fixed at one lace on the

plate, it could be located at a node of one or several modes included in the frequency band of interest. If this is the case, the mode will not appear, and the analysis will be incomplete. In order to overcome this problem, the accelerometer was fixed at the exact same location where the disturbance force was applied. Such a procedure ensures that the modes not being measured will not be excited by the force. In the previous modal analysis, the disturbance was fixed in space (Speaker in a corner of the cavity) and the pressure was measured at 300 locations in the cavity. In the case of the modal analysis of the plate, the sensor is fixed in space, but the excitation is applied at 192 different locations. Due to the principle of reciprocity, these two methods should provide similar results.

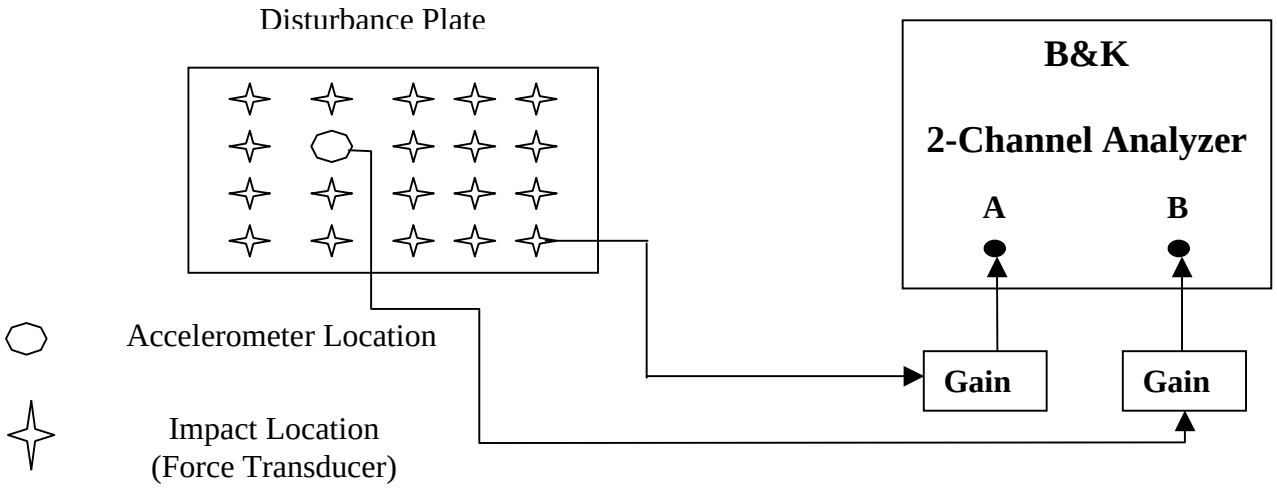

Figure 3.13 Modal analysis set-up.

Table 3.3 Set-up of the B&K analyzer

Measurement	Dual Spectrum Averaging
Channel A	Force Transducer
Channel B	Accelerometer
Trigger	Channel A, + slope 0.1(max input)
Delay	Trigger A –4.88 ms
Averaging	5
Frequency Spectrum	0-400Hz; ΔF=0.5 Hz T = 2S, ΔT=977μS
Weighting	Exponential Window, length 2s

A typical frequency response measured at point number 54, together with its coherence, is presented in Figure 3.14. Good coherence is obtained for data above 30 Hz. This shows that the data obtained are reliable at frequencies higher than 30 Hz. The results of the modal analysis conducted between 30 and 250 Hz are given in Table 3.4 and Figure 3.15. Nineteen modes have been found in the frequency band of interest. Details concerning resonance frequencies, damping, and shapes are given in Table 3.4. Modes (1,6) and (2,6) do not appear. This due to the accelerometer being located close to a node of these modes. As it has been explained earlier, the disturbance force will not excite these modes. Therefore these modes are of no importance in the analysis. The mode shapes presented in Figure 3.15 are similar in shape to those of a clamped plate. The first mode has one anti-node in the middle of the plate, mode 3 has three anti-nodes, etc. Modes 6 and 13 are not exactly the same as the modes of a clamped plate. The differences are due to the boundary conditions. The frequencies associated with these modes are not those of a clamped plate with the same characteristics either. The plate can not be assumed clamped to the rest of the test cavity.

The most interesting pieces of information for the finite element model are the mode shapes, since they provide the wavelength number of each mode for both the y and z direction. In the y-direction the highest wavelength number is 1.5 (mode 3,1 at 182 Hz; 3,2…), and 4.5 in the z-direction (mode 1,9 at 216 Hz), as illustrated in Figure 3.15. It can be concluded that the plate needs to be described by at least 9 by 3 elements. The model shown in Figure 3.7 has a density of 10 by 7 elements, which is sufficient to accurately describe the behavior of the plate below 250 Hz.

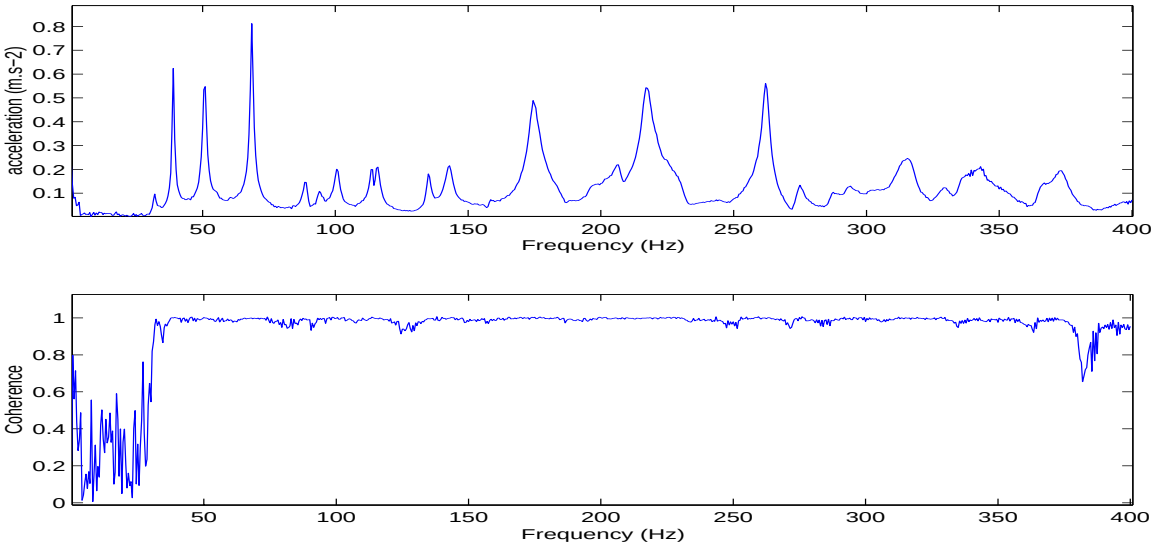

Figure 3.14 Example of a frf (H1) and its coherence.

Table 3.4 Natural frequencies and modal damping

Frequency (Hz)	Damping (e-3)	Mode Shape (m,n)	Frequency (Hz)	Damping (e-3)	Mode Shape (m,n)
31.8	6.8	1,1	156.8	5.3	2,5
38.6	5.7	1,2	172.8	6.4	1,8
49.9	8.5	1,3	182.1	5.5	3,1
67.2	5.0	1,4	196.9	9.7	3,2
87.2	4.5	1,5	207.3	6.8	3,3
94.9	5.3	2,1	216.8	8.6	1,9
100.5	7.3	2,2	220.2	9.8	2,7
114.9	6.68	2,3	230.4	6.7	3,4
134.8	7.3	2,4	247.1	6.0	2,8
143.5	6.2	1,7			

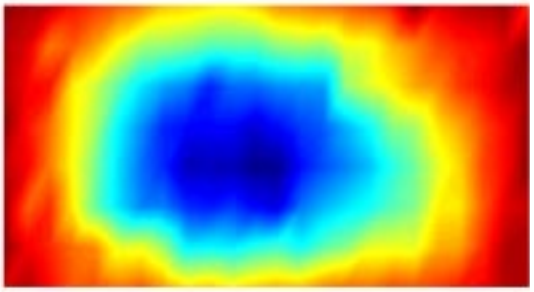

Mode 1 (31.8 Hz)

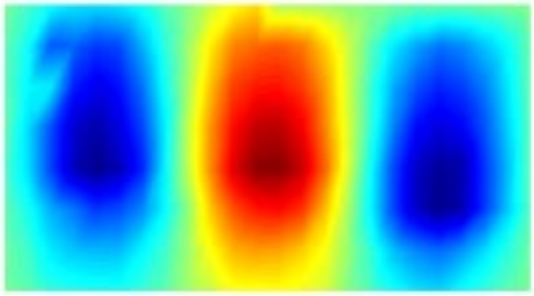

Mode 3 (49.9 Hz)

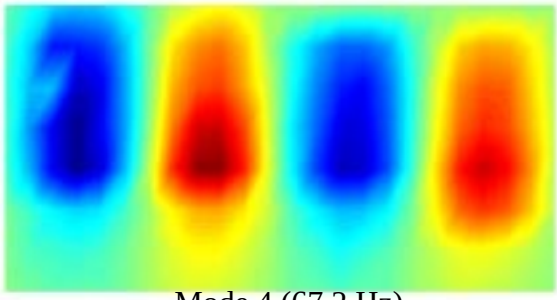

Mode 4 (67.2 Hz)

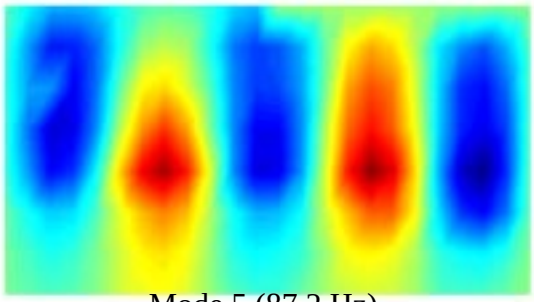

Mode 5 (87.2 Hz)

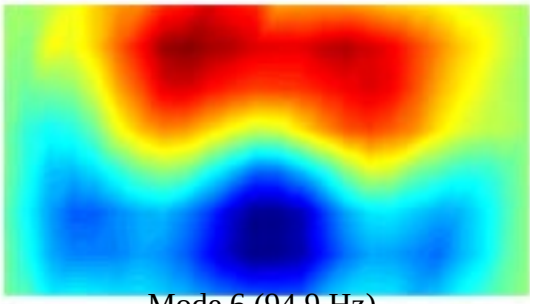

Mode 6 (94.9 Hz)

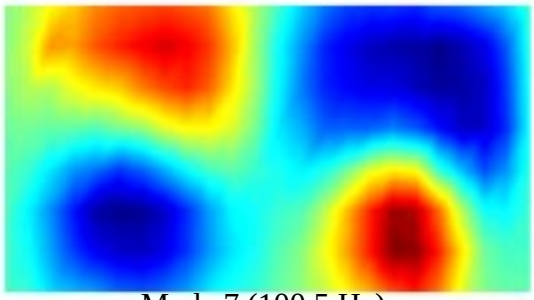

Mode 7 (100.5 Hz)

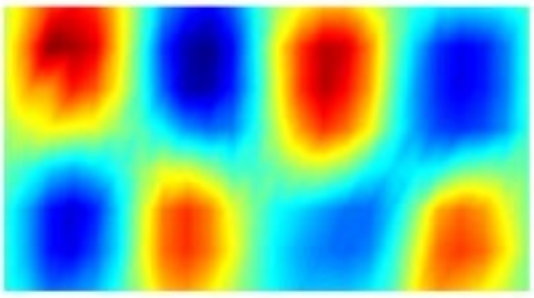

Mode 10 (143.5 Hz)

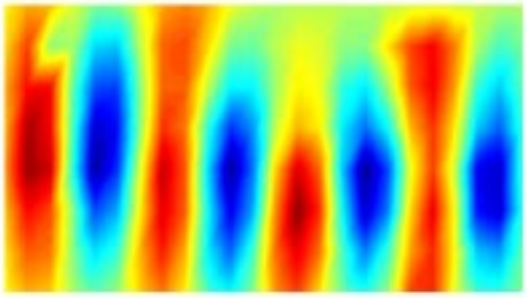

Mode 13 (196.7 Hz)

Figure 3.15 Structural mode shapes

3.2.2 Application to the Finite Element Model

The frequency response of the plate due to the input force of the shaker was measured at 70 locations on the plate, as discussed in the previous chapter. The locations of the data points coincide with the center of each surface element used in the finite element model used to describe the plate. Each of these surface elements vibrates independently, their velocity amplitude and phase being measured with the PCB laser vibrometer. Each surface element vibrates like a piston, i.e. its entire surface vibrates in phase and with the same amplitude.

In order to validate the structural-acoustic model, the following experiment has been undertaken. A white noise signal band passed between 40 and 250 Hz is amplified and input to the 50lb. shaker attached to the steel plate. The pressure field created by this disturbance is measured using the microphones mounted on the traverse as described in section 3.1.3. In Figure 3.16, the solid line represents the sum of the pressure squared measured in the test structure. The dashed line represents the same quantity predicted by the model. The global trend of the two curves is similar. However, some of the peaks in the model have less damping than in the experiment, particularly at 70, 115 and 170 Hz. The main problem with the model is that each element of the plate is independent. Therefore, the 'physical' continuity of the plate has not been taken into account. Figure 3.17 shows the discrete model against the actual displacement along the y-axis.

In conclusion, the model is accurate enough to provide a qualitative assessment of the acoustic field created by the disturbance in the frequency band of interest, but is not accurate enough to quantify the generated sound pressure levels. Regarding the simulations, this implies that only general trends and relative values (such as attenuation of the pressure level after active control) can be obtained.

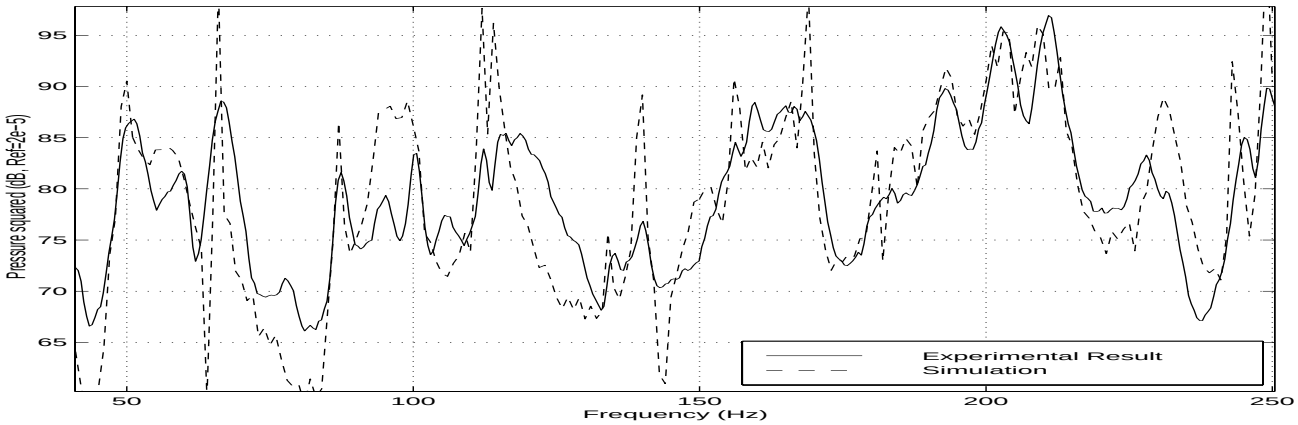

Figure 3.16 Pressure due to the disturbance plate

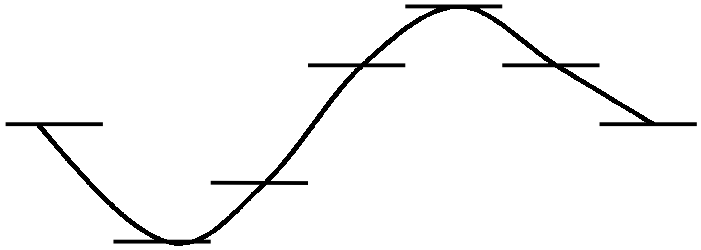

Figure 3.17 Discrete model of the plate in y-direction